magnetochemistry

MDPI

Article

AC Susceptibility Studies under DC Fields in Superspinglass Nanomaghemite-Multiwall Carbon Nanotube Hybrid

Juan A. Ramos-Guivar [1,*], F. Jochen Litterst [2,3] and Edson C. Passamani [4]

1 Grupo de Investigación de Nanotecnología Aplicada para Biorremediación Ambiental, Energía, Biomedicina y Agricultura (NANOTECH), Facultad de Ciencias Físicas, Universidad Nacional Mayor de San Marcos, Av. Venezuela Cdra 34 S/N, Ciudad Universitaria, Lima 01, Peru
2 Institut für Physik der Kondensierten Materie, Technische Universität Braunschweig, 38106 Braunschweig, Germany; j.litterst@tu-braunschweig.de
3 Centro Brasileiro de Pesquisas Físicas, Rio de Janeiro, RJ 22290-180, Brazil
4 Department of Physics, Federal University of Espírito Santo-UFES, Vitória, ES 29075-910, Brazil; passamaniec@yahoo.com.br
* Correspondence: juan.ramos5@unmsm.edu.pe; Tel.: +51-191-472-8212

Abstract: Magnetic properties of maghemite (γ-Fe_2O_3) nanoparticles grown on activated multiwall carbon nanotubes have been studied by alternating current (AC) magnetic susceptibility experiments performed under different temperatures, frequencies, and applied magnetic fields. Transmission electron images have suggested that the γ-Fe_2O_3 nanoparticles are not isolated and have an average size of 9 nm, but with a relatively broad size distribution. The activation energies of these 9 nm γ-Fe_2O_3 nanoparticles, determined from the generalized Vogel–Fulcher relation, are reduced upon increasing the direct current (DC) field magnitude. The large activation energy values have indicated the formation of a superspinglass state in the γ-Fe_2O_3 nanoparticle ensemble, which were not observed for pure γ-Fe_2O_3 nanoparticles, concluding that the multiwall carbon nanotubes favored the appearance of highly concentrated magnetic regions and hence the formation of superspinglass state. Magnetic relaxation studies, using Argand diagrams recorded for DC probe fields (<20 kOe) below the magnetic blocking temperature at 100 and 10 K, have revealed the presence of more than one relaxation process. The behavior of the ensemble of γ-Fe_2O_3 nanoparticles can be related to the superspinglass state and is also supported by Almeida–Thouless plots.

Keywords: AC susceptibility; magnetic nanoparticles; multiwall carbon nanotubes; magnetic relaxation; maghemite; superspinglass state

Citation: Ramos-Guivar, J.A.; Litterst, F.J.; Passamani, E.C. AC Susceptibility Studies under DC Fields in Superspinglass Nanomaghemite-Multiwall Carbon Nanotube Hybrid. *Magnetochemistry* **2021**, *7*, 52. https://doi.org/10.3390/magnetochemistry7040052

Academic Editor: Lotfi Bessais

Received: 21 February 2021
Accepted: 16 March 2021
Published: 12 April 2021

1. Introduction

Magnetic nanoparticles (NPs) are compelling materials from the fundamental and applied physical viewpoints [1–4]. Therefore, we have recently made efforts in preparing different nano-adsorbents using the co-precipitation method and inducing modifications on the nanoparticle surfaces with various inorganic and organic functional groups for potential use in heavy metals uptake from contaminated effluents [4–6]. Most important is the fact that the co-precipitation method allows size control of really small NPs, with mean particle sizes in the interval from 3 to 20 nm and with a relatively narrow particle size distribution (PSD).

On the other hand, the growth of the small NPs in different matrices is an additional challenge. In particular, novel magnetic effects may be expected to appear in zero-dimensional iron oxide nanoparticles dispersed in solid matrices. According to magnetic properties, at least, two noticeable magnetic effects disserve to be mentioned—(i) the significant reduction in saturation magnetization (M_s) values and/or (ii) the absence of a saturation regime even at high magnetic fields (5 T) [7]. These special properties are intrinsically related to high specific surface area and surface spin disorder configurations, yielding coexisting and competing magnetic effects, such as spin canting [7,8],

exchange bias [9], the formation of cluster glass (CG)/superspinglass (SSG) states [10], super-ferromagnetism [10], etc.

In a previous study, we demonstrated that the strong surface magnetic disorder present in γ-Fe_2O_3 NPs dispersed in mesoporous silica (SBA15) leads to a collective spin frustration [11], and a similar behavior was recently observed for Zn-substituted $Cu_{1-x}Zn_xFe_2O_4$ spinel ferrites [12]. Interparticle and intraparticle magnetic interactions are difficult to differentiate, and thus, these issues remain of great interest. Various magnetic techniques (bulk and local) and also distinct magnetic direct current (DC) and alternating current (AC) protocols are necessary to be employed to figure out the nature of the magnetic interactions in an ensemble of magnetic NPs dispersed in a specific magnetic matrix. In this context, cluster glass (CG) behavior or the formation of a superspinglass (SSG) state in NPs may have two origins that are under debate [7–11], which are (i) concentrated samples with strong dipolar interactions and (ii) surface effects due to high surface anisotropy and surface area that often lead to spin canted structures on the NPs surface. Furthermore, magnetic relaxation, a complex issue in nanomagnetism [10], can bring some information about the presence of interparticle interactions and the anisotropic energy barrier distribution, directly related to the physical phenomena involved in magnetically blocked NPs with broad PSD [13]. For example, the superparamagnetic relaxation regime has been well studied, using Mössbauer spectroscopy and AC susceptibility measurements [10,11,13]. However, magnetic relaxation effects are complex phenomena in an ensemble of magnetic NPs and, therefore, they require a much more systematic magnetic study, sometimes with the necessity of application of protocols often not available in laboratories. Some relaxation studies have been reported for [MnR_4TPP][TCNE] and lanthanide-based single-molecule magnets [14,15].

Regarding matrices into which magnetic NPs are dispersed, carbon nanotubes (CNTs) and multiwall carbon nanotubes (MWCNTs) are outstanding materials with remarkable mechanical, electrical, catalytic, and adsorptive properties. The MWCNTs are formed by multilayers of CNTs that lend these materials a high specific surface area and reactive catalytic sites. Therefore, the CNT multilayers can chemically be activated and functionalized with -COO- and -NH_2 groups [16]. As reported in the literature, the surface functionalization of MWCNTs with metals can be achieved by three methods—(i) electrochemical, (ii) chemical, and (iii) physical methods [16]. Obviously, all these metal nanotube hybrids will have different properties that will depend on particle sizes and their distributions within the nanotube cavities [17,18].

Nanosized metal oxides (NMOs), such as nanosized ferric oxides, manganese oxides, aluminum oxides, titanium oxides, magnesium oxides, have a high surface area and chemical affinity for heavy metals uptake from the aqueous environment and wastewater [19]. By combining the NMOs with MWCNTs, an enhancement in the adsorptive and magnetic properties can be obtained. In particular, the recent applications of magnetic NPs, functionalized NMOs, and solid magnetic matrices have also been employed for oil-water separation [20–22]. By magnetizing the oil with magnetic nanopowders, the oil can easily be covered and then separated magnetically with a permanent magnet. For a fully controlled performance of the adsorptive mechanism in a magnetic remediation process, the above magnetic NPs effects must be first understood. To our best knowledge, there is a lack in the literature related to the study of magnetic relaxation processes of magnetic NPs functionalized in the MWCNTs (NPMWCNTs).

The importance of these basic physical aspects for the application of nanohybrid magnetic Fe-oxide NPs grown on an MWCNTs matrix (nanohybrid NPMWCNTs) has been the motivation for the here reported study using transmission electron microscopy (TEM), energy dispersive X-ray analysis (EDX), and a complete AC susceptibility characterization also under DC probe fields. The generalized Vogel–Fulcher relation was employed to determine the activation energies that are related to interactive magnetic spin clusters/superspin moments with a collective freezing behavior. Argand diagrams at 100 and 10 K were plotted to study the relaxation phenomena below the Fe-oxide magnetic blocking temperature.

The results have shown the presence of more than one relaxation process and relaxation times associated with interacting NPs with broad PSD, as shown by TEM images.

2. Results and Discussions

2.1. Transmission Electron Microscopy (TEM) and Energy Dispersive X-ray (EDX) Analysis

The TEM images for the pure MWCNTs and nanohybrid NPMWCNTs are respectively shown in Figure 1a,b. The morphologies of the NPMWCNTs are not changed when compared with those found in the MWCNTs, i.e., there are no surface morphology changes of CTNs due to the dispersion of Fe-oxide NPs (mean sizes of 9 nm) [4]. The TEM image of the nanohybrid NPMWCNTs also suggested that the Fe NPs are relatively close, and as will be discussed, this observation will favor a specific magnetic state for the ensemble of the Fe-oxide NPs in the MWCNTs matrix. Regarding the functionalization process, it should be mentioned that the Fe-oxide NPs are anchored to the MWCNTs by the carboxyl groups available on the surface, previously activated by a specific acid activation process, as demonstrated by infrared studies [4], μ-Raman, and X-ray photoelectron spectroscopy (XPS) [23].

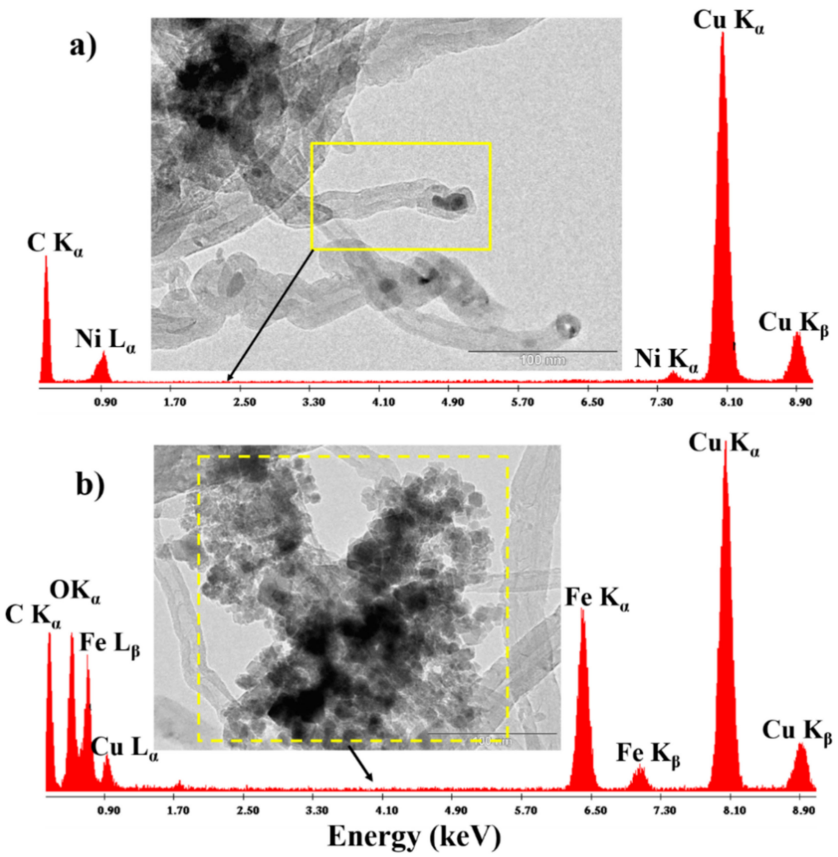

Figure 1. Energy dispersive X-ray analysis-transmission electron microscopy (EDX-TEM) images of the (**a**) multiwall carbon nanotubes (MWCNTs) and (**b**) magnetic NPs functionalized in the MWCNTs (NPMWCNTs). Bar length of 100 nm for both TEM images.

The EDX quantitative analysis for the pure MWCNTs has shown the presence of an atomic percentage of 4.1% for Ni, as metallic traces coming from the chemical vapor deposition (CVD) technique. As we reported in our previous study [4], the activated MWCNTs have an insignificant ferromagnetic signal due to Ni, which has a maximum magnetic moment of 0.4 emu/g. This value is really small when comparing with the functionalized MWCNTs with nanomaghemite, which show a M_s value of 37 emu/gFe. Hence, we are assuming that there is not a significant implication or modification of the magnetic properties of the functionalized hybrid due to Ni impurities. In addition, no other

impurities were registered in the MWCNTs with a total atomic percentage of carbon of 95.9%. After functionalizing the MWCNTs with the Fe-oxide NPs, the EDX image, shown in Figure 1b, has revealed only elements of C, O, and Fe, with atomic percentages of 32.7%, 43.5%, and 23.8%, respectively. It indicates the formation of magnetic Fe-oxide NPs on the MWCNTs; this is supported by X-ray diffraction, Raman, and XPS analysis [23].

2.2. Superspinglass Phase Analysis

Before entering into a discussion of the AC magnetic susceptibility (χ) protocols, we briefly summarize our previous DC magnetic studies reported in [4]. Under an applied magnetic field of 80 Oe, a maximum of susceptibility was observed at 237 K upon zero-field cooling (ZFC) and field cooling (FC) measurements and preliminarily attributed to the PSD. On the other hand, the hysteresis *M(H)* curves have revealed a non-saturated behavior even for an applied field of 4 T, and that results in a value of M_S of 37 emu/gFe (smaller than the value for pure nanomaghemite, which is close to 60 emu/gFe) [4]. This reduction of the M_s value is intrinsically related either to surface effects or interparticle magnetic interactions in the sample. Both effects generally would lead to spin disorder favoring spin-glass-like configurations. Therefore, those results have suggested that it still is necessary to study the dynamic properties to fully understand the magnetic behavior of the MWCNTs with the Fe-oxide NPs [24].

The temperature dependence of the in-phase (χ′(T,f)) and out-of-phase (χ′(T,f)) magnetic susceptibilities under zero DC field for the nanohybrid NPMWCNTs are displayed in Figure 2a,b. Moreover, to gain additional information about the activation energies and magnetic relaxation process of our ensemble of Fe-oxide NPs, we have evaluated the response of the AC susceptibility for selected DC fields (Figure 3). The χ′(T) and χ″(T) curves show broad maxima reflecting the broad PSD of our ensemble. The temperature with the maximum value of susceptibility is labeled as T_M. As can be seen in Figure 3a–d T_M shifts to lower temperatures. Thus, according to the Arrhenius-like expression (Equation (1)), it will have a frequency dependence arising from the dynamic magnetic behavior of the nano-ensemble. If the sample is monodispersed, T_M can be assumed as the blocking temperature of the nano-ensemble. However, if a broad PSD is predominant, the χ′(T) and χ″(T) curves will also depict a broad signal. A nice explanation about the currently accepted definition of the blocking temperature can be found in reference [25].

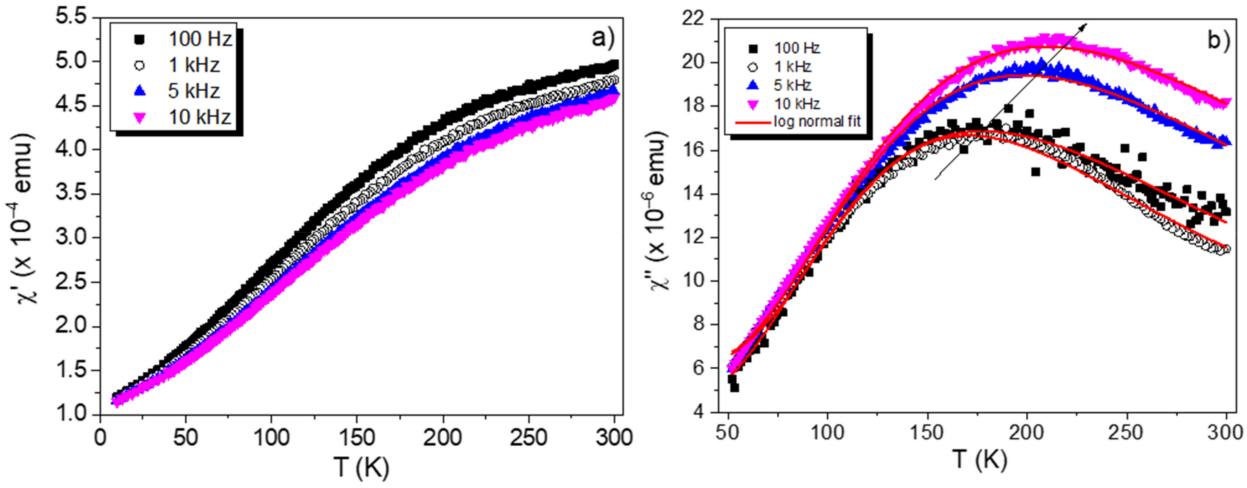

Figure 2. In-phase χ′ (**a**) and out-of-phase χ″ (**b**) components of the AC magnetic χ for zero DC external magnetic field.

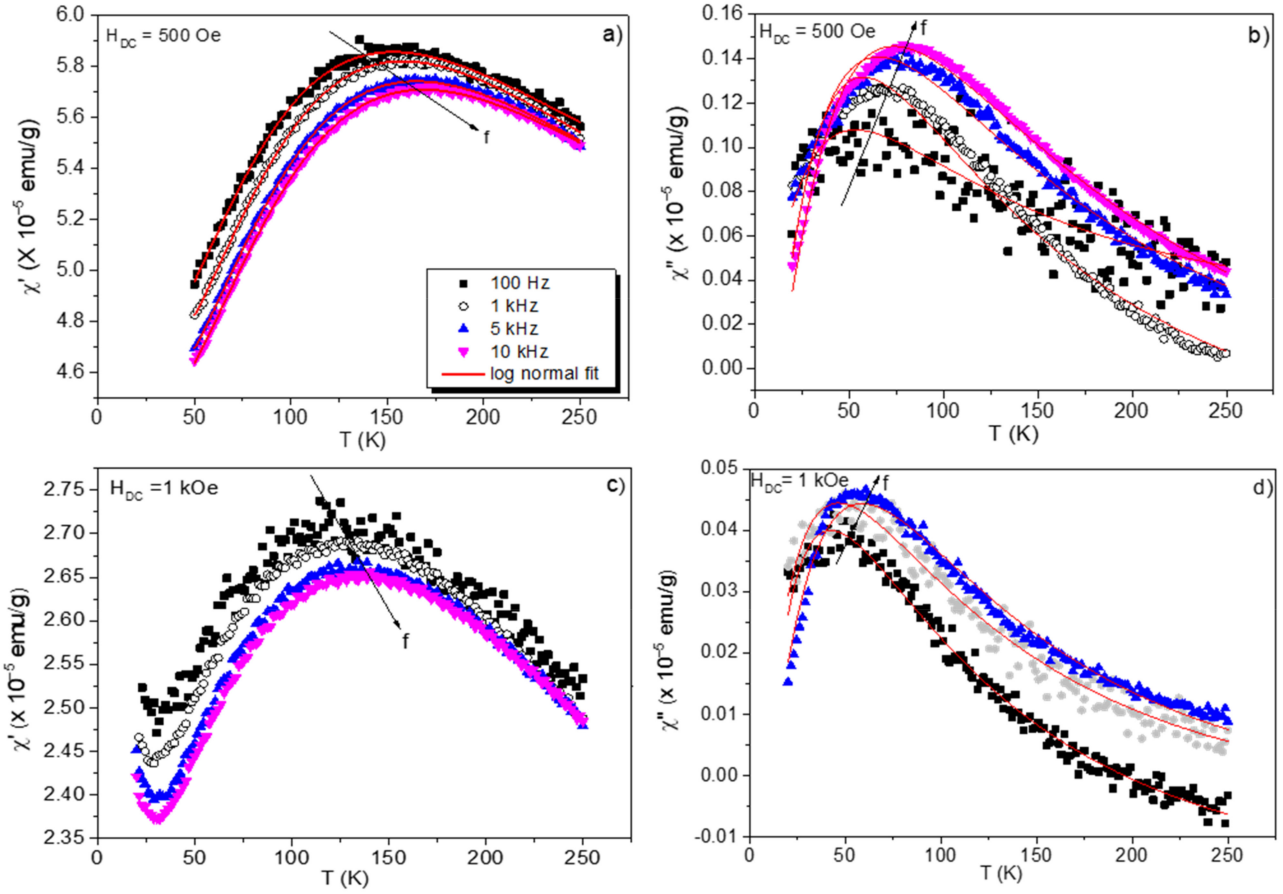

Figure 3. Selected AC magnetic susceptibilities (χ'(T,f) (**a**)–(**c**) and χ''(T,f) (**b**)–(**d**)) recorded under two DC bias fields (0.5 and 1 kOe) and for different frequencies. The full lines correspond to the fittings of the data using log-normal distribution.

The behavior of the χ'(T,f) curves is commonly found in cases of magnetic NPs with sizes bigger than 10 nm, where, on the one hand, the χ'(T,f) curves show an increase as the sample temperature rises to values close to room temperature (RT). On the other hand, the χ''(T,f) component displays a broad maximum with a particular frequency behavior. Here, we must mention that posterior analysis by Vogel–Fulcher (V–F) law and Almeida–Thouless (A–T), the AC magnetic χ (under different DC bias fields) will have a dependence on the zero-field data; therefore, it is appropriated (in case of nanohybrids with a broad PSD) for a reasonable analysis to take the χ''(T) signal that allows calculating the T_M values. In particular, we have observed an increment in the T_M when the frequency increases from 100 Hz (216 K) to 10 kHz (294 K). It is well established that in an ensemble of superparamagnetic NPs with no magnetic interaction, the magnetic relaxation time is calculated using the Arrhenius-like expression given by [26,27] as follows:

$$\tau = \tau_o e^{\frac{KV}{k_B T_M}} \quad (1)$$

where $\tau = \frac{1}{f}$, $E_a = KV$ is the anisotropy energy barrier, K is the anisotropy constant, V is the TEM particle volume, k_B is Boltzmann's constant (1.38×10^{-23} JK^{-1}), and τ_o is the characteristic time, which is found in the range from 10^{-13} s to 10^{-9} s. Applying Equation (1), we have found an unrealistic value of $\tau_o = 10^{-24}$ s, suggesting that the Fe-oxide NPs are magnetically interacting. Therefore, to account for interparticle magnetic interactions, we have used the linearized Vogel–Fulcher (V–F) law [11], which is more appropriate,

$$T_M \ln\left(\frac{\tau}{\tau_0}\right) = \frac{KV}{k_B} + T_0 \ln\left(\frac{\tau}{\tau_0}\right), \quad (2)$$

where E_a = KV is the activation energy and T_0 is related to the interparticle magnetic interactions. A linear fit using the V–F law (Equation (3)), for non-zero DC bias field was applied, and taking $\tau_0 = 10^{-9}$ s, has yielded the following fitting parameters: T_0 = 59.5 (4) K and an intersection value of $\frac{E_a}{k_B}$ = 2.24(5) × 10^3 K. We would first like to stress that the τ_0-parameter is related to the dynamic properties of the magnetic nano-ensemble. Then, it is expected that for a narrow PSD (ideal superparamagnetic regime), the magnetic relaxation will be faster and times of 10^{-11} and 10^{-13} s are expected. On the other hand, for a broad PSD (our case), the slow and intermediate relaxations are predominant and fluctuation times are higher, and usually in the interval of 10^{-6} s to 10^{-9} s [24,25]. This justifies the value of $\tau_0 = 10^{-9}$ s chosen for modeling the dynamic behavior of the magnetic nanohybrid. Now, we have to mention that canonical cluster-spin-glass systems should have a value of $\frac{E_a}{k_B} < 2T_f$. However, in our case, this value is higher than ~11T_f, where T_f is the spin freezing temperature. Such large activation energies were reported in other nanosystems with SSG states [24,28]. Thus, the here obtained values are suggesting that the behavior of our system also reflects interactive magnetic spin clusters/superspin moments with collective freezing.

To enforce the last argument, we have made the use of the relative variation of the T_M values, estimated from the χ″ (T,f) curve per decade of the applied frequency, that supplies more details of the magnetic state of the sample, as given by the following empirical parameter [27]:

$$ø = \frac{\Delta T_M}{T_M \Delta \log_{10}(f)}. \quad (3)$$

Its value ranges from 0.05 to 0.18 [11,27,29] if the system is in the cluster-spin-glass-like regime, but ø~0.3–0.5 is assigned for an ideal superparamagnetic state [27,29]. From our data, recorded in the interval of 100 Hz to 10 kHz, we have obtained a mean ø-value of 0.13, reinforcing the characteristics of the cluster-spin-glass-like system of our magnetic nanohybrid NPMWCNTs.

Equation (3) was also applied to calculate the E_a for each different (see V–F plots and linear fits in Figure 4a–d) applied field, and the obtained fitted values are reported in Table 1. From these values, we noticed that the activation energy decreases as the DC fields increases. This is in agreement with other studies related to molecular magnets [14,30]. The inflection points of the χ curves can be understood as the transition from a magnetically fast fluctuating state to a static ordered phase. In our case, it refers to the freezing of the SSG state that occurs due to the interparticle magnetic interactions. This magnetic state can be attributed to being due to (i) dipolar magnetic interactions in this magnetically concentrated system and (ii) non-collinear spin structures of the Fe-oxide NPs bound in the MWCNTs surfaces. Additionally, the ø-values, obtained under DC fields, have slightly varied between 0.03 and 0.05, supporting the presence of a collective SSG phase in our system.

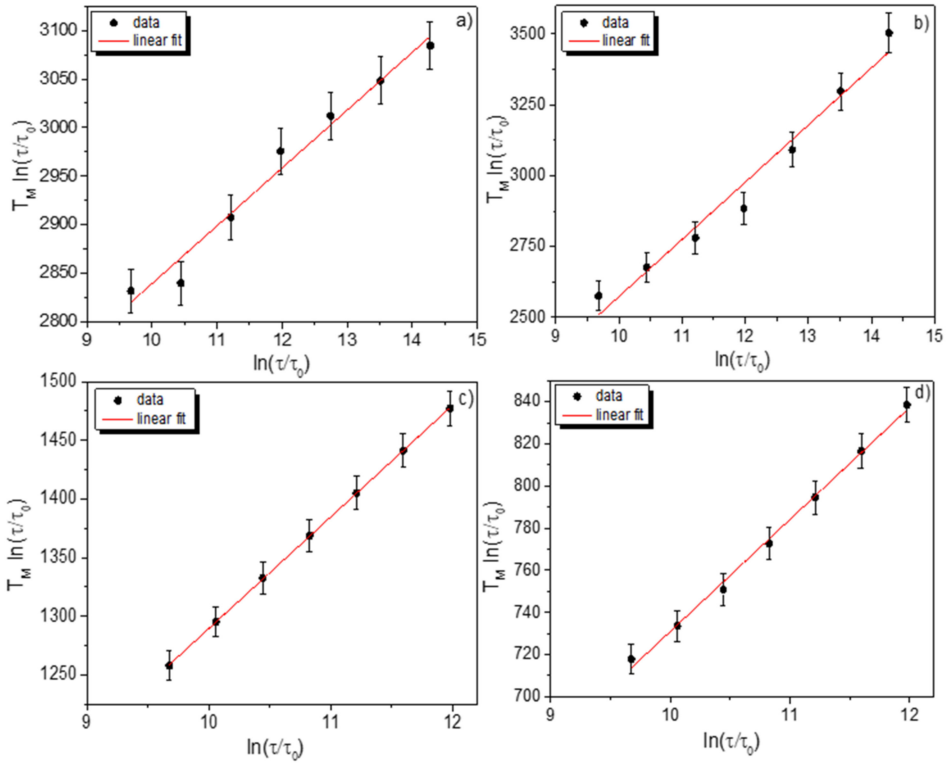

Figure 4. Vogel–Fulcher (V–F) plots under DC fields of (**a**) 0 Oe; (**b**) 0.5 kOe (**c**) 1 kOe and (**d**) 2 kOe T_M values were determined from χ″(T) curves and for different frequencies. The full lines represent the result of the fits of the experimental data obtained from the AC magnetic χ curves recorded under different DC fields.

Table 1. Values of the T_0, and $\frac{E_a}{k_B}$ parameters obtained after fitting the dependence of the T_M for χ″(T) curves recorded under several DC fields using the V–F relation.

H_{DC} (Oe)	T_0 (K)	$\frac{E_a}{k_B}$ (K)
0	59.5 (4)	2244 (5)
500	202 (5)	556 (5)
1000	95 (3)	338 (4)
2000	53 (1)	199 (4)

2.3. Almeida-Thouless Plot

To gain a deeper insight into the magnetic behavior, χ″(T,f) measurements were made under different DC magnetic fields (0 to 2 kOe). The χ″(T,f) curves have a broad maximum that depends on the magnetic field intensity (the temperature in which the T_M has shifted to low temperatures as the applied magnetic field has increased). In particular, the T_M values, in the interval of 273 to 72 K for 0 to 2 kOe, were obtained for an applied frequency of 5 kHz. The same tendency was observed for lower frequencies. The values of T_M are related to the broad PSD and the presence of strongly interacting particles. Figure 5a,b displays the dependence of the magnetic field with T_M, and as can be noticed, no linear behavior is observed. The mean-field framework suggests that the SSG state at low fields can be studied by the A–T curve, using the following relation [31,32]:

$$H(T) = H_0\left(1 - \frac{T_M}{T_f}\right)^p, \quad (4)$$

where the parameters H_0 (field amplitude) and p can be obtained by fitting the experimental data (it brings information about the magnetic state and properties of the system). In addition, it should be stressed that the A–T diagram delimitates the superparamagnetic

(SPM) to SSG phase transition. According to Figure 5, it is in fact seen that the T_M value decreases with the increase of H-field and the fitting of the H vs. T_M data, using Equation (4), gives close parameters of p = 1.8 (2), T_f = 248 (2) K and H_0 = 3.6 (3) kOe for 1 and 5 kHz. The values of R^2 = 0.995 indicate the good fitting by Equation (4) and the above values, obtained from the fits, also support the presence of the SSG phase in our sample [32].

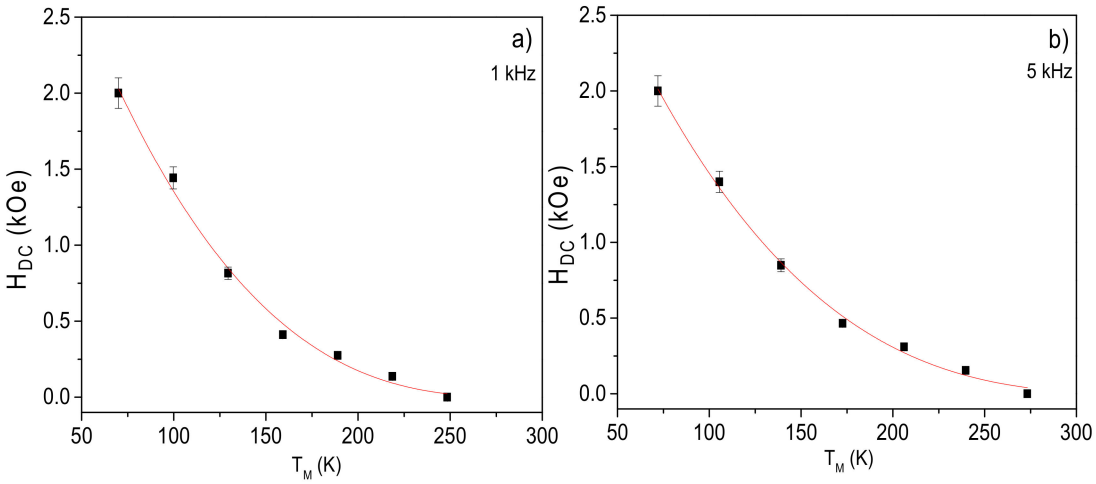

Figure 5. Almeida–Thouless (A–T) plots for 1 kHz (**a**) and 5 KHz (**b**). T_M values were taken from the χ''(T,f) component of the AC susceptibility curves under several DC field values.

It needs to be stressed that pure γ-Fe_2O_3 NPs, synthesized by chemical co-precipitation route [10], did not present the mentioned SSG state, despite it exhibited agglomerated regions that, in principle, would also cause significant magnetic interparticle interactions. On the other hand, our researches focused on growth and functionalization processes of γ-Fe_2O_3 NPs in mesoporous (SBA-15, TEM mean size of 10.5 nm) [11] and recently in microporous zeolite type 5A (TEM mean sizes of 8.7 to 9.4) [33]. It has been shown that the SSG state is strongly favored by the more concentrated magnetic regions found in this type of magnetic nanohybrids. Thus, according to the present results, the activated MWCNTs can also be favoring the SSG state. Consequently, we would infer that magnetic NPs dispersed and concentrated in mesoporous matrices could lead to an SSG state below T_f, as a consequence of the matrix effect.

2.4. Argand Diagrams

Often magnetic relaxation is studied by thermoremanent (TRM) measurements, showing an exponential-like dependence of the magnetic moment with time and the SSG transition temperature may be observed in samples with the strong surface disorder and significant interparticle magnetic interactions [11,21]. Another useful method to analyze the magnetic spin relaxation phenomena in magnetic NPs is Argand diagrams [14,15]. If a complete semicircle is observed in the Argand diagram (recorded for a fixed temperature and DC applied field), one can conclude that the ensemble of magnetic NPs has a narrow PSD, and consequently only one single relaxation process is expected [13]. On the other hand, if there is a broad PSD with some magnetic interaction, the χ'(T,f) versus χ''(T,f) Argand diagram will show an incomplete semicircle-like feature, assigned to the distribution of relaxation times and anisotropy energies. For our nanohybrid NPMWCNTs, the dependence of the χ'(T,f) and χ''(T,f) susceptibilities were studied as a function of the frequency, at a fixed temperature and DC field (field values smaller than 20 kOe). The χ'(T,f) components of the magnetic susceptibility vs. widened frequencies window (from 0.1 to 10 kHz) at 100 K and 10 K are presented in Figure 6a,b. We can clearly notice that the χ'(T,f) decreases with frequency, and the χ''(T,f) revealed a small order of 10^{-8} emu/g (figure not shown), as would be expected in magnetic nano-ensembles [10]. The effect of the DC

field causes a significant reduction in the χ″(T,f) signal that is represented by a flattened semicircle (T = 10 K).

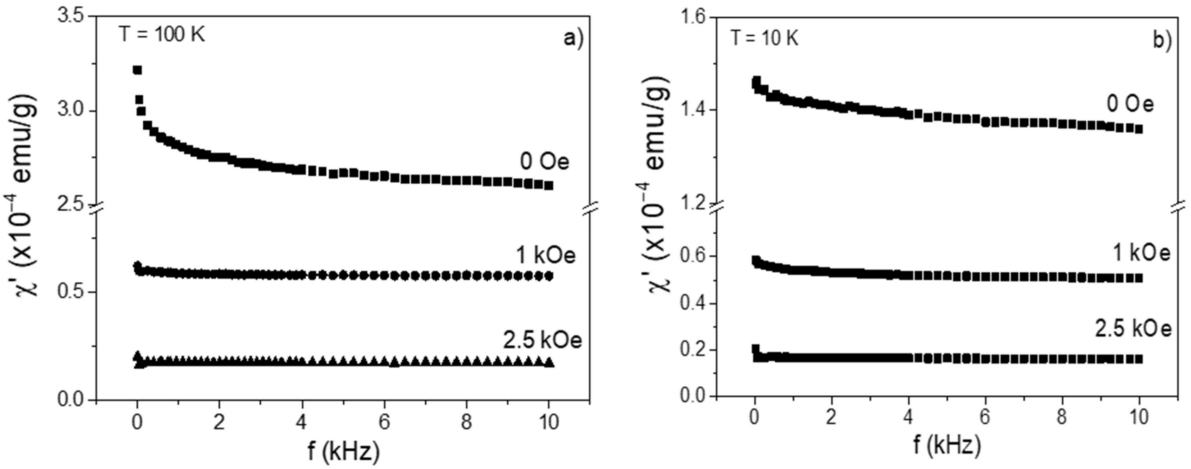

Figure 6. Frequency dependence of the χ′ (T,f) component recorded at 100 K (**a**) and 10 K (**b**) under selected DC bias field.

The Argand diagrams for NPWNCTs nanohybrid in Figure 7a–d were obtained by measuring the frequency dependence of the χ′(T,f) and χ″(T,f) susceptibilities. Two temperatures (100 K and 10 K) were used for interpretation of the magnetic relaxation process. The first selected temperature is below and close to the T_M values of the Fe-oxide NPs, whereas the second temperature is close to the total blocking magnetic state of the sample (SSG state). At 100 K, only half of an ideal semicircle for the χ′(T,f) vs. χ″(T,f) diagram is observed. The lack of a non-perfect semicircle for the χ′(T,f) vs. χ″(T,f) diagram can be explained assuming that at 100 K, there is a distribution of relaxation times of the ultrafast spin relaxation process related to a broad PSD, as suggested by TEM results and also previously demonstrated by Mössbauer study performed for the NPMWCNTs [23]. In the study, using a Blume–Tjon two-level relaxation model, we have concluded that the ultra-fast spin relaxation (Néel relaxation) process starts to occur at 80 K, and the spin–spin relaxation is intrinsically related to the freezing temperature of the SSG state with the transition from under-barrier to over-barrier fluctuations. Spin–spin relaxation phenomena have also been studied in concentrated samples with strong dipolar interactions that also cause the formation of an SSG state [10,11]. The observed distribution of relaxation times reflects a distribution of energy barriers caused by the mentioned PSD, uncompensated Fe^{3+}–spins at the particle surface [8,23], and interparticle magnetic interactions, as reported in the literature [10,11,32].

At 10 K, when the ensemble of the Fe-oxide NPs is in the SSG state, the Argand plots are flattened, meaning that more than one magnetic relaxation process is present [13–15]. With increasing field, the maximum of the semicircle increases and the semicircle is more pronounced. This observation indicates that even at 10 K, the distribution of relaxation times is still present, which is again compatible with a broad PSD, as observed by TEM images and concluded from Mössbauer spectroscopy [23].

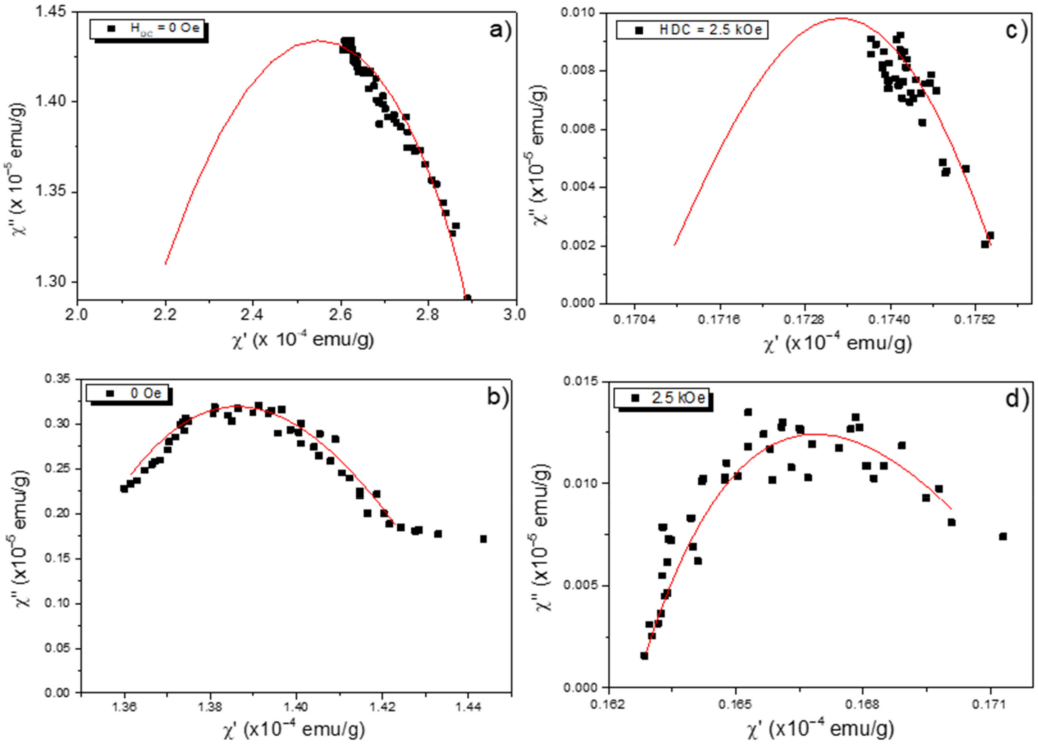

Figure 7. Argand diagrams recorded at 100 K (above) and 10 K (below) for zero applied (**a**,**b**) and DC field of 2.5 kOe (**c**,**d**).

3. Materials and Methods

Synthesis and Magnetic Characterization

The synthesis of the nanohybrid NPWMCNTs (9 nm γ-Fe_2O_3 NPs +MWCNTs) is fully described in reference [23]. Briefly, the maghemite NPs were grown on MWNCTs by co-precipitation method in a highly alkaline medium (pH = 12). A detailed study of structural properties by Raman spectroscopy of the nanohybrid NPWMCNTs is available in reference [23]. TEM experiments were performed in a JEM-2000 FX (JEOL Ltd., Tokyo, Japan) and the imaging interpretation was performed using Image J software (National Institutes of Health Bethesda, MD, USA). EDX spectra were recorded in some TEM images for quantitative analysis. $\chi'(T,f)$ and $\chi''(T,f)$ components of the AC magnetic χ were obtained using a commercial Quantum Design Physical Properties Measurement System, Evercool-II setup (Quantum Design North America, San Diego, CA, USA), using the AC Measurement System option. The χ data were obtained in a temperature range from 4 to 300 K, with an AC probe field of 10 Oe, different DC applied fields (<20 kOe), and for an interval of frequency from 1 to 10 kHz. To obtain the Argand diagrams, we first fixed the temperature and an applied field value (<20 kOe) and then recorded $\chi'(T,f)$ and $\chi''(T,f)$ values varying frequency from 1 Hz to 10 kHz. A step Δf of 150 Hz was used up to 1 kHz and 250 Hz for higher frequency values. The data for the Argand plots of the nanohybrid NPWMCNTs were obtained at 10 and 100 K (i.e., below the magnetic blocking temperature).

4. Conclusions

The nanohybrid NPMWCNTs (γ-Fe_2O_3 NPs + MWCNTs) prepared by co-precipitation were systematically studied using several AC magnetic χ protocols. TEM analysis shows that (i) the γ-Fe_2O_3 NPs have sizes of 9 nm, (ii) there is a large PSD dispersed in the MWCNTs, and (iii) the ensemble of Fe-oxide NPs is relatively concentrated. AC magnetic χ in the absence and in the presence of DC fields has brought information about the magnetic dynamic behavior of the ensemble of the Fe-oxide NPs. In general, the magnetic results of different protocols have first suggested that the SSG state is the magnetic state of the nanohybrid 9 nm NPMWCNTs. This magnetic SSG state is explained assuming

a strongly dipolar interaction among the Fe-oxide NPs in our magnetic concentrated ensemble, not observed in pure γ-Fe_2O_3 NPs. For example, the results of the V–F law show a ø-parameter value of 0.05, which matches with values found for an SSG state. Magnetic relaxation was studied based on the Argand diagrams recorded at temperatures of 100 K and 10 K (below the magnetic blocking temperature) for different applied DC fields. These diagrams also indicate a system of strongly interacting magnetic NPs with a distribution of relaxation times associated with the broad PSD, as determined from TEM. We have then been able to show that there is a significant contribution from the mesoporous matrix in the magnetic state of magnetically concentrated NPs that would lead, in general, to a formation of the SSG state accompanied by a slight reduction of the M_S value.

Author Contributions: Conceptualization, J.A.R.-G., E.C.P., and F.J.L.; methodology, J.A.R.-G., E.C.P., and F.J.L.; software, J.A.R.-G.; validation, J.A.R.-G., E.C.P., F.J.L.; and J.A.R.-G.; investigation, J.A.R.-G., E.C.P., and F.J.L.; resources, J.A.R.-G., E.C.P., and F.J.L.; data curation, J.A.R.-G.; writing—original draft preparation, J.A.R.-G.; writing—review and editing, J.A.R.-G., E.C.P., and F.J.L.; visualization, J.A.R.-G., E.C.P., and F.J.L.; supervision, J.A.R.-G., E.C.P., and F.J.L.; project administration, J.A.R.-G.; funding acquisition, J.A.R.-G. and F.J.L. All authors have read and agreed to the published version of the manuscript.

Funding: The authors thank to the Fondo Nacional de Desarrollo Científico, Tecnológico y de Innovación Tecnológica (FONDECYT-CONCYTEC), project number 177-2020-FONDECYT, UFES and FAPES, CNPq for financial supports.

Data Availability Statement: The original data related to this research can be asked any time to the corresponding author's email: juan.ramos5@unmsm.edu.pe.

Conflicts of Interest: The authors declare no conflict of interest.

References

1. Kheirkhah, P.; Denyer, S.; Bhimani, A.D.; Arnone1, G.D.; Esfahani, D.R.; Aguilar, T.; Zakrzewski, J.; Venugopal, I.; Habib, N.; Gallia, G.L.; et al. Magnetic Drug Targeting: A Novel Treatment for Intramedullary Spinal Cord Tumors. *Sci. Rep.* **2018**, *8*, 11417. [CrossRef]
2. Saleem, H.; Zaidi, S.J. Recent Developments in the Application of Nanomaterials in Agroecosystems. *Nanomaterials* **2020**, *10*, 2411. [CrossRef]
3. Khan, F.S.A.; Mubarak, N.M.; Khalid, M.; Walvekar, R.; Abdullah, E.C.; Mazari, S.A.; Nizamuddin, S.; Karri, R.R. Magnetic nanoadsorbents'potential route for heavy metals removal—A review. *Environ. Sci. Pollut. Res.* **2020**, *27*, 24342–24356. [CrossRef]
4. Guivar, J.A.R.; Sadrollahi, E.; Menzel, D.; Fernandes, E.G.R.; López, E.O.; Torres, M.M.; Arsuaga, J.M.; Arencibia, A.; Litterst, F.J. Magnetic, structural and surface properties of functionalized maghemite nanoparticles for copper and lead adsorption. *RSC Adv.* **2017**, *7*, 28763. [CrossRef]
5. Guivar, J.A.R.; Bustamante, A.; Gonzalez, J.C.; Sanches, E.A.; Morales, M.A.; Raez, J.M.; López-Muñoz, M.J.; Arencibia, A. Adsorption of arsenite and arsenate on binary and ternary magnetic nanocomposites with high iron oxide content. *Appl. Surf. Sci.* **2018**, *454*, 87–100. [CrossRef]
6. Ramos-Guivar, J.A.; Taipe, K.; Schettino Jr, M.A.; Silva, E.; Torres, M.A.M.; Passamani, E.C.; Litterst, F.J. Improved removal capacity and equilibrium time of maghemite nanoparticles growth in zeolite type 5A for Pb(II) adsorption. *Nanomaterials* **2020**, *10*, 1668. [CrossRef]
7. Morales, M.P.; Veintemillas-Verdaguer, S.; Monteo, M.I.; Serna, C.J.; Roig, A.; Casas, L.L.; Martínez, B.; Sandiumenge, F. Surface Internal spin canting in γ-Fe_2O_3 nanoparticles. *Chem. Mater.* **1999**, *11*, 3058–3064. [CrossRef]
8. Ramos-Guivar, J.A.; López, E.O.; Greneche, J.M.; Litterst, F.J.; Passamani, E.C. Effect of EDTA organic coating on the spin canting behavior of maghemite nanoparticles for lead (II) adsorption. *Appl. Surf. Sci.* **2021**, *538*, 148021. [CrossRef]
9. Phan, M.-H.; Alonso, J.; Khurshid, H.; Lampen-Kelley, P.; Chandra, S.; Repa, K.S.; Nemati, Z.; Das, R.; Iglesias, O.; Srikanth, H. Exchange Bias Effects in Iron Oxide-Based Nanoparticle Systems. *Nanomaterials* **2016**, *6*, 221. [CrossRef]
10. Bedanta, S.; Kleemann, W. Superparamagnetism. *J. Phys. D Appl. Phys.* **2009**, *42*, 013001. [CrossRef]
11. Ramos-Guivar, J.A.; Krohling, A.C.; López, E.O.; Litterst, F.J.; Passamani, E.C. Superspinglass behavior of maghemite nanoparticles dispersed in mesoporous silica. *J. Magn. Magn. Mater.* **2019**, *485*, 142–150. [CrossRef]
12. Akhter, S.; Hakim, M.A.; Hoque, S.M.; Das, H.N. Disorder magnetic behavior of Zn-substituted $Cu_{1-x}Zn_xFe_2O_4$ spinel ferrites. *Solid State Commun.* **2021**, *326*, 114181. [CrossRef]
13. Zhang, X.X.; Wen, G.H.; Xiao, G.; Sun, S. Magnetic relaxation of diluted and self-assembled cobalt nanocrystals. *J. Magn. Magn. Mater.* **2003**, *261*, 21–28. [CrossRef]

14. Balanda, M. AC susceptibility studies of phase transitions and magnetic relaxation: Conventional, Molecular and Low-Dimensional Magnets. *Acta Phys. Pol. A* **2013**, *124*, 964–976. [CrossRef]
15. Gonzalez, J.F. Isotopic Enrichments of Lanthanide Based Single Molecule Magnets. Ph.D. Thesis, Université Rennes 1, Rennes, France, 2019.
16. Peng, H.-X. *Multifunctional Polymer Nanocomposites, Chapter 8: Polyurethane Nanocomposite Coatings for Aeronautical Applications*; CRC Press: Cleveland, OH, USA, 2011; p. 361, ISBN 978-1-4398-1682-0.
17. Cunha, C.; Panseri, S.; Iannazzo, D.; Piperno, A.; Pistone, A.; Fazio, M.; Russo, A.; Marcacci, M.; Galvagno, S. Hybrid composites made of multiwalled carbon nanotubes functionalized with Fe_3O_4 nanoparticles for tissue engineering applications. *Nanotechnology* **2012**, *23*, 465102. [CrossRef]
18. Demir, A.; Baykal, A.; Sözeri, H.; Topkaya, R. Low temperature magnetic investigation of Fe_3O_4 nanoparticles filled into multiwalled carbon nanotubes. *Synth. Met.* **2014**, *187*, 75–80. [CrossRef]
19. Hua, M.; Zhang, S.; Pan, B.; Zhang, W.; Lv, L.; Zhang, Q. Heavy metal removal from water/waste water by nanosized metal oxides: A review. *J. Hazard. Mater.* **2012**, *211–212*, 317–331. [CrossRef]
20. Muniz, E.P.; de Assuncao, L.S.D.; de Souza, L.M.; Ribeiro, J.J.K.; Marques, W.P.; Pereira, R.D.; Porto, P.S.S.; Proveti, J.R.C.; Passamani, E.C. On cobalto ferrite production by sol-gel from orange fruit residue by three related procedures and its application in oil removal. *J. Clean. Prod.* **2020**, *265*, 121712. [CrossRef]
21. Fossati, A.; Alho, M.M.; Jacobo, S.E. Covalent functionalized magnetic nanoparticles for crude oil recovery. *Mater. Chem. Phys.* **2019**, *238*, 121910. [CrossRef]
22. Zhang, J.; Shao, Y.; Hsieh, C.-T.; Chen, Y.F.; Su, T.-C.; Hsu, J.-P.; Juang, R.-S. Synthesis of magnetic iron oxide nanoparticles onto fluorinated carbon fabrics for contaminant removal and oil-water separation. *Sep. Purif. Technol.* **2017**, *174*, 312–319. [CrossRef]
23. Ramos-Guivar, J.A.; Gonzalez-Gonzalez, J.C.; Litterst, F.J.; Passamani, E.C. Rietveld refinement, μ-Raman, XPS, and Mössbauer studies of metal oxide—Nanoparticles growth on multiwall carbon nanotubes and graphene oxide. *Cryst. Growth Des.* **2021**. [CrossRef]
24. Aslibeiki, B.; Kameli, P.; Salamati, H.; Eshraghi, M.; Tahmasebi, T. Superspin glass state in $MnFe_2O_4$ nanoparticles. *J. Magn. Magn. Mater.* **2010**, *322*, 2929–2934. [CrossRef]
25. Bruvera, I.J.; Zélis, P.M.; Calatayud, M.P.; Goya, G.F.; Sánchez, F.H. Determination of the blocking temperature of magnetic nanoparticles: The good, the bad, and the ugly. *J. Appl. Phys.* **2015**, *118*, 184304. [CrossRef]
26. Shtrikman, S.; Wohlfarth, E.P. The theory of the Vogel-Fulcher law of spin glasses. *Phys. Lett. A* **1981**, *85*, 467–470. [CrossRef]
27. Dormann, J.I.; Bessais, L.; Fiorani, D. A dynamic study of small interacting particles: Superparamagnetic model and spin-glass laws. *J. Phys. C Solid State Phys.* **1988**, *21*, 2015–2034. [CrossRef]
28. Khurshid, H.; Lampen-Kelley, P.; Iglesias, O.; Alonso, J.; Phan, M.; Sun, C.-J.; Saboungi, M.-L.; Srikanth, H. Spin-glass-like freezing of inner and outer surface layers in hollow γ-Fe_2O_3 nanoparticles. *Sci. Rep.* **2015**, *5*, 15054. [CrossRef]
29. Fertman, E.; Dolya, S.; Desnenko, V.; Beznosov, A.; Kajňaková, M.; Fecher, A. Cluster glass magnetism in the phase-separated $Nd_{2/3}Ca_{1/3}MnO_3$ perovskite. *J. Magn. Magn. Mater.* **2012**, *324*, 3213–3217. [CrossRef]
30. Balanda, M.; Tomkowicz, Z.; Haase, W.; Rams, M. Single-chain magnet features in 1D [MnR_4TPP][TCNE] compounds. *J. Phys. Conf. Ser.* **2011**, *303*, 012036. [CrossRef]
31. Zhang, Y.D.; Budnick, J.I.; Hines, W.A.; Chien, C.L.; Xiao, J.Q. Effect of magnetic field on the superparamagnetic relaxation in granular Co-Ag samples. *Appl. Phys. Lett.* **1998**, *72*, 2053. [CrossRef]
32. Suzuki, M.; Fullem, S.I.; Suzuki, I.S.; Wang, L.; Zhong, C.-H. Observation of superspin-glass behavior in Fe_3O_4 nanoparticles. *Phys. Rev. B* **2009**, *79*, 024418. [CrossRef]
33. Ramos-Guivar, J.A.; Passamani, E.C.; Litterst, J. Superspinglass state in functionalized zeolite 5A-maghemite nanoparticles. *AIP Adv.* **2021**, *11*, 035223. [CrossRef]